Semiconductor Clusters in the Sol-Gel Process: Quantized Aggregation, Gelation, and Crystal Growth in Concentrated ZnO Colloids

Lubomir Spanhel* and Marc A. Anderson

Contribution from the Water Chemistry Program, University of Wisconsin, Madison, Wisconsin 53706. *Received May 31, 1990. Revised Manuscript Received October 19, 1990*

Abstract: A new synthesis of ZnO wurtzite clusters (crystallite sizes 3-6 nm) is presented. This novel approach, employing ultrasound, allows one to produce relatively highly concentrated 0.1 M Q-ZnO colloids within a few minutes. These colloids remain in a dispersed state for weeks. They can be further concentrated into stable syruplike liquids (molarities of ~1 M). Under the extreme concentration conditions (10 M Q-ZnO colloids) employed, ZnO alcogels are formed, and self-induced crystal growth occurs in the alcogels (sizes ranging between 1 and 5 mm). Furthermore, the small crystallites can be cast on porous or nonporous supports and fired to obtain ZnO ceramic membranes and thin films. All ZnO materials investigated were colorless and did not opalesce, while they exhibited a bright luminescence when exposed to UV light. Progressive concentration from dilute sols to the compact crystal state produced structured luminescence excitation spectra with magic maxima ranging from 250 and 400 nm. In dilute suspensions, excitonic transitions in "primary" clusters can be observed. In concentrated suspensions, additional excitonic levels appear, attributed to the appearance of primary cluster aggregates. Gelation and crystal growth produce further excitonic levels. This process is explained as a growth of secondary cluster aggregates. One can destroy the crystals in an ultrasound field followed by dilution of the alcogels until the original spectroscopic properties from primary clusters are restored. An electronic correlation diagram and crystal growth mechanism, both based on aggregation, are proposed.

Introduction

Research on semiconducting Q materials (Q, showing quantum mechanical effect of exciton confinement) has been increasingly popular in many scientific and industrial communities. Reviews concerning small-particle research,[1] cluster quantum mechanics,[2] and optics of quantum wires and dots[3] summarize the current state of the art in this new branch of physical chemistry. Two main findings of this research should be emphasized. First, the density of electronic states decreases and the band gap energy increases as the particles become smaller and smaller. Second, an occurrence of structure (resolved excitonic transitions) and hypsochromic shifts in optical absorption and luminescence spectra are noted. These are general observations made within the size domain spanning molecular and bulk crystalline properties.

At present, interest in sol-gel technology is growing as well.[4,5] This interdisciplinary science explores the synthesis and properties of ceramic and biological materials, covering the entire size scale encountered during processing, from the earliest stages through to the final desired product. In small-particle research, powerful spectroscopic techniques are used to study highly dilute one-component colloids containing isolated particles. In sol-gel science, particle-particle interactions and their related aggregation phenomena become the main event. Small-angle scattering of neutrons,[6] X-rays,[7] and visible photons[8] by concentrated colloids is studied to describe the aggregate structure and to understand the conditions under which aggregates are formed.

Recently we have used CdS clusters (particle diameter <5 nm) to prepare optically transparent phosphate-ordered xerogels (giant cluster aggregates) with unusual mechanical properties.[9] Luminescence spectroscopy (LS) studies showed that during the sol-gel transition, even very small clusters tend to aggregate. They did not fuse or reprecipitate to give large clusters. A similar conclusion has been drawn in synthesis studies on silicate-ordered luminescing gels composed of ZnS-CdS or Ag_2S-CdS clusters.[10]

In the present paper, we address the synthesis of sol-gel-based ZnO materials in the following sequence: 3-nm clusters → syrups → gels → 5-mm crystals. Again, we applied LS technique to follow changes in electronic properties during the transition from highly dilute sols to compact crystals. This study was possible as it is known that bulk ZnO crystals[11] as well as low-concentration ZnO colloids[12,13] luminesce. We note reversible activation of structured excitation spectra as a result of straightforward cluster consolidation. We further show that large ZnO crystals can be grown at ambient laboratory conditions using the ZnO gels. CVD[14] and hydrothermal[15] techniques have been developed to grow high-purity ZnO crystals. Chemical spray,[16] PE-MO-CVD,[17] and PHOTO-MOCVD[18] have also been suggested to fabricate oriented and epitaxial ZnO thin films. To the best of our knowledge, however, a sol-gel-based approach for the synthesis of ZnO crystals and films has not been reported.

Experimental Section

Apparatus. Steady-state photoluminescence measurements were performed with a SLM 500C spectrofluorometer. Spectra from all ZnO materials under investigation were recorded and corrected. Variable-angle front surface accessories were used. Fresh quinine sulfate dihydrate solutions (in 0.1 N sulfuric acid) were employed in luminescence quantum yield determinations. UV-vis spectra were recorded with a Varian DMS-80 spectrophotometer. Spectra from colloidal suspensions were obtained with 1-cm quartz cells.

ZnO cluster sizes were determined by transmission electron microscopy (100 kV, JEOL 100CX); 300-mesh copper grids coated with Formvar were used to prepare the TEM samples.

* To whom correspondence should be addressed. Present address: Hahn-Meitner-Institute Berlin, Glienicker Str. 100, 1000 Berlin 39, Germany.

(1) (a) Henglein, A. *Top. Curr. Chem.* **1988**, 143, 115-180; (b) *Chem. Rev.* **1989**, *89*, 1861-1873, and references therein.
(2) (a) Brus, L. E. *J. Phys. Chem.* **1986**, *90*, 2555. (b) Bawendi, M.; Steigerwald, M. L.; Brus, L. E. *Annu. Rev. Phys. Chem.* **1990**, *41*.
(3) Kash, K. J. *Luminescence* **1990**, *46*, 69-82.
(4) Hench, L. L.; West, J. K. *Chem. Rev.* **1990**, *90*, 33-72.
(5) Brinker, C. J.; Scherer, G. W. *Sol-Gel Science*; Academic Press, Inc.: New York, 1990; and references therein.
(6) Ramsey, J. D. F. *Chem. Soc. Rev.* **1986**, *15*, 335-371.
(7) Kratky, O. *Prog. Colloid Polym. Sci.* **1988**, *77*, 1-14.
(8) Hackley, V. A.; Anderson, M. A. *Langmuir* **1989**, *5*, 191-198.
(9) Spanhel, L.; Anderson, M. A. *J. Am. Chem. Soc.* **1990**, *112*, 2278.
(10) Spanhel, L.; Anderson, M. A., unpublished results.
(11) Beutel, E.; Kutzelnigg, A. *Monatsch. Chem.* **1932**, *61*, 69.
(12) Koch, U.; Fojtik, A.; Weller, H.; Henglein, A. *Chem. Phys. Lett.* **1985**, *122*, 507.
(13) Bahnemann, D. W.; Kormann, C.; Hoffmann, M. R. *J. Phys. Chem.* **1987**, *91*, 3789.
(14) (a) Matsumoto, K.; Shimaoka, G. *J. Cryst. Growth* **1988**, *86*, 410. (b) Matsumoto, K.; Konemura, K.; Shimaoka, G. *J. Cryst. Growth* **1985**, *71*, 99.
(15) Croxall, D. F.; Ward, R. C. C.; Wallace, C. A.; Kell, R. C. *J. Cryst. Growth* **1974**, *22*, 117.
(16) Cossement, D.; Streydio, J. M. *J. Cryst. Growth* **1985**, *72*, 57.
(17) Shimizu, M.; Matsueda, Y.; Shiosaki, T.; Kawabata, A. *J. Cryst. Growth* **1985**, *71*, 209.
(18) (a) Shimizu, M.; Kamei, H.; Tanizawa, M.; Shiosaki, T.; Kawabata, A. *J. Cryst. Growth* **1988**, *89*, 365; (b) **1989**, *94*, 895.

0002-7863/91/1513-2826$02.50/0

X-ray measurements were performed on a Scintag, Inc. PAD V diffraction system and on a STOE automated diffraction system (Stoe & Cie GmbH). X-ray patterns from powder samples were taken in reflection mode. The diffraction patterns from colloidal samples were detected by applying fast-transmission diffractometry using position-sensitive detectors, and Debay-Scherrer capillaries.

Optical microscopic investigations of the ZnO crystals were performed on a Diaphot-TMD inverted microscope (Nikon, Nippon Kogaku K.K.). Bright- and dark-field optics including polarization accessories were used.

Synthesis. Fabrication of Q-ZnO materials involves three major steps: (1) preparation of organometallic precursor containing 0.1 M Zn, (2) preparation of nearly stoichiometric 0.1 M ZnO colloids, and (3) solvent removal by rotary evaporation (conditions: 12 Torr, 25 °C) to concentration levels resulting in desired products such as syrups and alcogels.

(1) Organometallic Zn Precursor. Zinc acetate ($C_4H_6O_4Zn{\cdot}2H_2O$ from Aldrich) and absolute ethanol (200 proof) were used as received without further purification. The precursor was made as follows: 0.5 L of ethanol containing 0.1 M Zn^{2+} was placed into a distillation apparatus fitted so that one could run the reaction under ambient atmospheric pressure, avoid moisture exposure, and collect condensate (1-L flask, a column with calcium chloride trap, an adapter, and a condensate receiver). Over a period of ~180 min, the solution was boiled at 80 °C and stirred with a magnetic stirring bar. At the end of this procedure, 0.3 L of condensate and 0.2 L of hygroscopic reaction mixture (in which precipitation occurred on the addition of a small amount of water) were obtained. NMR, CIR-FTIR, and UV–vis spectroscopic investigation of both fractions revealed that the reaction mixture contained a zinc compound containing acetic acid derivatives. A more detailed investigation of the reaction mechanism and the structure of this precursor will be presented separately.

(2) ZnO Clusters. The hygroscopic product (0.2-L quantity from the initial step) was placed into an Erlenmeyer flask and diluted to yield 0.5 L of ethanolic solution containing 0.1 M Zn^{2+}. Next, 0.14 M $LiOH{\cdot}H_2O$ powder (from Alfa Products) was added to the ethanolic solution. Finally, the suspension was placed into an ultrasonic bath in order to destroy the weakly soluble powder. This procedure accelerates the release of OH ions, resulting in immediate reaction to form a stable ZnO cluster solution. This process, performed at 0 °C and under air conditions, took 10 min. Room-temperature preparation gave slightly larger particles. Use of NaOH and KOH pellets, as well as $Mg(OH)_2$ powder, all gave turbid precipitates. The use of different alcohols (methanol and 2-propanol) and zinc salts (formate and citrate) to prepare highly concentrated ZnO colloids has been unsuccessful to date. Since the reactants were not ultrapure, glass fiber filters (0.1 μm pore size) were used to clean the cluster solutions before using them in concentration studies.

(3) Crystal Growth. Crystal growth in alcogels is, in most cases, a self-induced process occurring at room temperature. However, the growth rate, shape, and size of the crystals depended strongly upon the amount of LiOH used, e.g., the reaction stoichiometry. A rough pH measurement based stoichiometry test was made. In this test,three different ethanolic ZnO colloids were prepared by adding three different amounts of LiOH powder to the precursor solution containing 0.1 M Zn^{2+}. Then, a few drops of the resulting colloids were added to ultrapure water to give 5×10^{-3} M (with respect to zinc) stable colloids, and the pH was measured. Titration of ZnO colloids has demonstrated that the pH of the zero point of charge is ~9.[13] Thus, 0.1 M LiOH gave positively charged clusters (pH ≈ 6.5), 0.2 M LiOH gave negatively charged clusters (pH ≈ 10.5), and 0.14 M LiOH gave near-neutral clusters pH ≈ 8.2. In the last case, where nearly stoichiometric conditions governed the process, large trapezoids and rodlike crystals were grown in ethanolic 10 M gels over a period of 12 h. However, cotton-ball-like crystallite aggregates were created in a vacuum desiccator (12 Torr over zeolites) over a period of 5 days, when 0.1 M LiOH was used to prepare the colloid (Zn in relatively large excess). Colloids prepared from 0.2 M LiOH were not stable for a long time. Concentrating these cluster solutions to 10 M results in precipitation after 2 h, giving acicular, needlelike solids.

Results and Discussion

Primary Clusters. Figure 1 shows X-ray diffraction fingerprints of two ZnO powder samples isolated from a 10-min-old colloid (dashed line) and a 5-day-old colloid (solid line). In the fresh colloid, the diffraction peaks are broader, the ⟨002⟩ reflection appears to be a shoulder while the ⟨102⟩ reflection is slightly shifted to larger Bragg angles. After aging (after 5 days), the diffraction peaks were more intense and narrower, while the ⟨002⟩ reflection became a peak, indicating increased crystallinity. The spacing values and relative intensities of the peaks coincide with the JCPDS data, so the observed patterns can be unambiguously

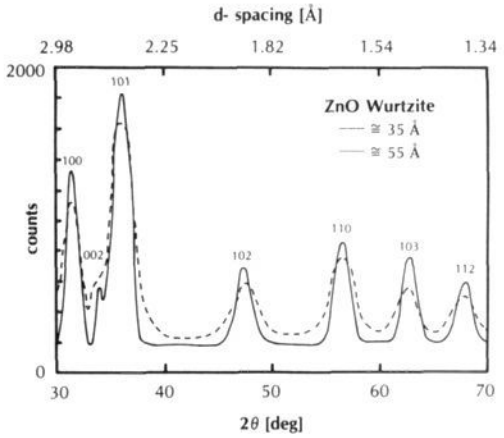

Figure 1. X-ray powder patterns of ZnO crystallites isolated from a fresh (dashed line) and an aged (solid line) ZnO colloid.

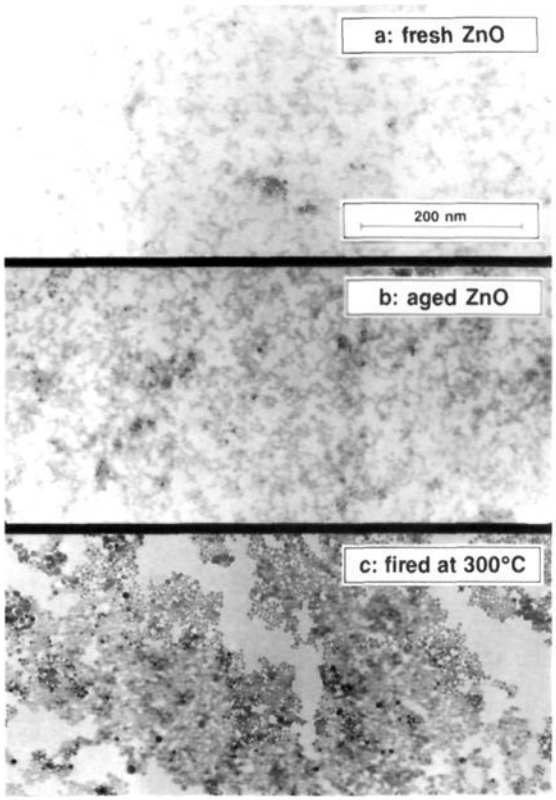

Figure 2. Transmission electron micrographs of ethanolic ZnO colloids: (a) fresh colloid sample, (b) aged colloid sample, (c) ZnO monolayer after firing at 300 °C.

attributed to the presence of hexagonal wurtzite crystallites. By application of the Scherrer–Warren formula,[19] the average crystallite size was calculated to be ≃3.5 nm in fresh colloids and ≃5.5 nm in 5-day-old ones.

Figure 2 shows transmission electron micrographs from the above investigated samples. One recognizes a spherical shape of the ZnO clusters. The cluster size distribution has been determined to be relatively narrow in both fresh (part a, diameters of ~3.5 nm) and 5-day-old colloids (part b, diameters of ~5.5 nm). Firing at 300 °C does not effect ZnO cluster size (part c, average diameter of ~6 nm).

Small-angle neutron-scattering studies on ZnO have been recently performed. The gyration radius of the ZnO clusters has been determined to be 1.7 nm in a freshly prepared colloidal

(19) West, A. R. *Solid State Chemistry and Its Applications*; John Wiley & Sons: New York, 1984; pp 174–175.

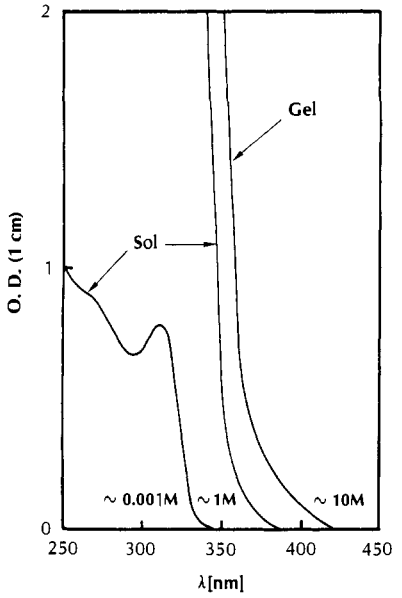

Figure 3. Changes in optical density of ZnO accompanying the transition from fresh sol to viscous sol to reversible alcogel. The UV–vis onsets are labeled with the corresponding molarities. Colloid preparation occurred at 0 °C.

sample. This coincides very well with the above calculated X-ray and TEM crystalline sizes.

Primary Aggregation Events. Figure 3 depicts the concentration dependence of the ZnO absorption spectrum as observed during sol–gel processing with fresh ethanolic colloids. Below 0.003 M, the UV–vis spectrum shows one 320-nm peak and a shoulder at 275 nm, attributed to exciton transitions in small ZnO clusters. Above 0.003 M, the colloids are characterized by a steep unstructured absorption curve. Its onset shifts to longer wavelengths as the molarity increases. One molar colloids have the consistency of "oily" liquids. They start to absorb at 380 nm. Optically transparent ZnO gels of 10–15 M do not flow. The bathochromic shift in the UV–vis spectrum of such materials is even more pronounced.

It is known from previous studies[12,13,20] that aging of alcoholic ZnO colloids produces larger particles and leads to bathochromic shifts in UV–vis and luminescence emission spectra. In UV–vis studies on 2-propanolic ZnO colloids Bahnemann et al.[13] noted that the aging is a reaction-controlled process, and that the bathochromic spectral shifts decrease linearly when plotted on a logarithmic time scale.

The effects of aging and "forced" cluster consolidation on the luminescence properties of ZnO are shown in Figure 4 (excitation spectra) and Figure 5 (corresponding emission spectra). The excitation spectrum of a fresh 0.001 M colloid (solid line) shows two maxima at 275 and 320 nm coinciding with the observed structure in UV–vis spectrum (Figure 3). Concentrating the sol to 1 M (solvent removal by rotary evaporation) activated an additional intense excitonic transition at 350 nm, as indicated by arrow A in Figure 4. On the other hand, after the fresh sample aged at room temperature over a period of 5 days, its less intense red-shifted excitation spectrum (arrow B) showed two bands at 315 and 350 nm, indicating development of large particles. Subsequent concentrating of the aged sol intensified the 350-nm peak and produced a new excitonic transition at 370 nm (arrow C). As seen in Figure 5, the emission band peaking at 500 nm shifted to 560 nm after aging. The concentration increase in both samples did not change the frequency spectrum of emitted photons while it did raise the luminescence quantum yield (absorbance corrected) from 0.2 to 0.4 as determined on fresh sols.

It is of note that dilution of both concentrated samples restores the original spectroscopic properties, implying that the forced

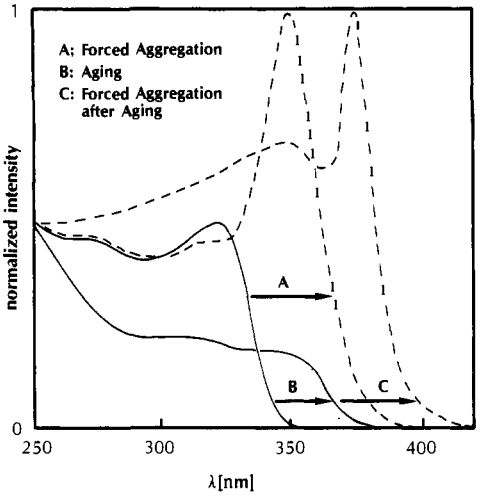

Figure 4. Comparison between a fresh and an aged ZnO colloid in a concentration/dilution experiment. Excitation spectra (emission wavelength independent) were obtained from dilute 0.001 M samples (solid lines) and from concentrated 1 M samples (dashed lines). Spectra were detected at 550 nm and are normalized at 250 nm.

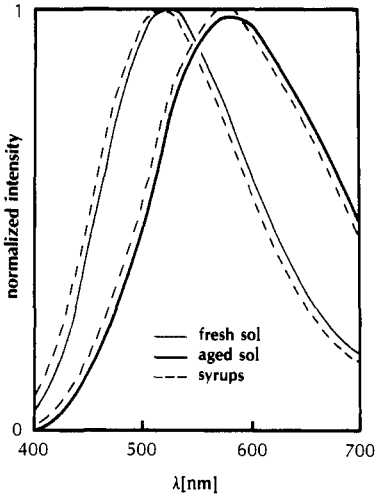

Figure 5. Luminescence emission spectra (excitation wavelength independent) from a fresh and an aged ZnO in dilute state (solid lines) and concentrated syruplike state (dashed lines); generated at λ_{ex} = 320 nm, normalized to the scale.

cluster consolidation does not involve the formation of covalent bonds with resulting changes in primary crystalline size. Second, as determined in fast-transmission diffractometry measurements on ZnO colloids, the line broadening remains unchanged as the molarity increases from 0.1 to 2 M. The observed X-ray transmission patterns from colloidal samples are the same as the X-ray diffraction patterns from powder samples isolated from fresh and aged colloids (see Figure 1), respectively. Third, both aging and forced concentrations have the same effect on samples with respect to the appearance of the 350-nm excitonic state.

A more detailed insight into the reversible consolidation is presented in Figure 6, which shows the evolution of excitation spectra during this process. As the molarity increases from 0.001 to 0.005 M, the excitation onset shifts to red. The intensity of the transitions into excitonic states increases, their energetics being unchanged (normalized). At 0.01 M and above, a shoulder appears, which then turns into a pronounced peak. The continuous bathochromic shift and increasing exciton oscillator strength finally reach a limit at 1 M, since a further increase in molarity does not produce further changes.

With the following formula[6]

$$L_{cc} \simeq c_p^{-1/3} \simeq 16R(V_M c_M)^{-1/3} \quad (1)$$

the average cluster–cluster separation length L_{cc} was calculated

(20) Haase, M.; Weller, H.; Henglein, A. *J. Phys. Chem.* **1988**, *92*, 482–487.

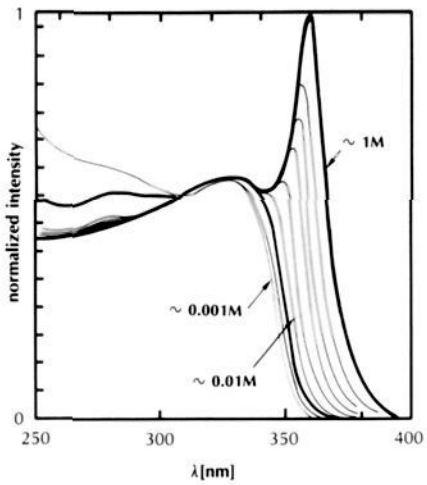

Figure 6. Room-temperature luminescence excitation spectra (detected at λ_{em} = 480 nm, normalized at 325 nm) from ZnO (prepared at 25 °C) of different concentrations ranging between 0.001 and 1 M.

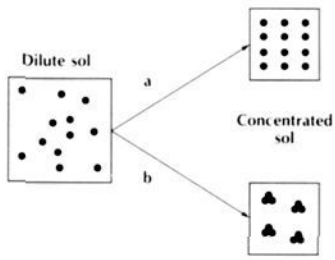

Figure 7. Diagram depicting two possible particle arrangements that can occur as the colloid is being concentrated.

by assuming the presence of smooth, spherical, and fully dense particles (c_p is the particle concentration, R is the particle radius, V_M is the molar volume, and c_M is molarity). With 0.01 M, one can calculate that at a distance of 15 particle diameters there is already a noticeable change in electronic properties (see Figure 6).

The question now arises as to which of the two particle arrangements in Figure 7 can better explain the observed spectroscopic changes. Route a would consider diffusion-limited collisional processes over distances of at least 15 particle diameters. It was calculated that such processes would require encounter lifetimes of several tens of microseconds. This is much longer than the typical ZnO colloid luminescence lifetime of ~100 ns. Thus, the clusters must be aggregated already in apparently dilute colloids, as described by alternative route b. It seems that during these primary aggregation events the primary clusters tend to achieve one particular arrangement; e.g., only certain aggregate sizes are abundant. With this argument one could understand why the bathochromic spectral shifts are strongly retarded (the energy of the excitation onset in Figure 6 decreases linearly when plotted on a logarithmic molar concentration scale) and why the observed excitation spectra are structured. These effects become more pronounced in supersaturated colloids, as we shall observe when secondary aggregation events occur.

From previous studies on CdS it is known that the presence of smaller and larger particles in a colloid can be recognized in a luminescence spectrum by varying the detection conditions.[1] The question arises as to whether it is possible to distinguish between isolated and aggregated ZnO clusters in electronic spectra. In other words, one might propose that the smaller particles are simply aggregates composed of primary clusters. As emphasized in Figures 4 and 5, the luminescence spectra of highly dilute 0.001 M and highly concentrated 1 M colloids are independent of detection wavelength. However, this is not observed for concentrations between these extremes. Figure 8 shows the result of a luminescence measurement performed on a fresh 0.5 M ZnO sol. First, a direct recombination of photogenerated electron–hole pairs

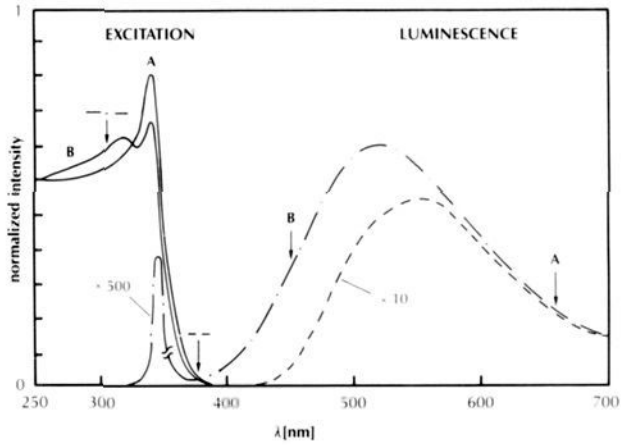

Figure 8. Electronic properties of a fresh 0.5 M ZnO sol. Luminescence excitation spectra (solid lines A and B) detected at 650 and 450 nm. Emission spectra (dash–dot and dashed lines) generated at 320 and 380 nm.

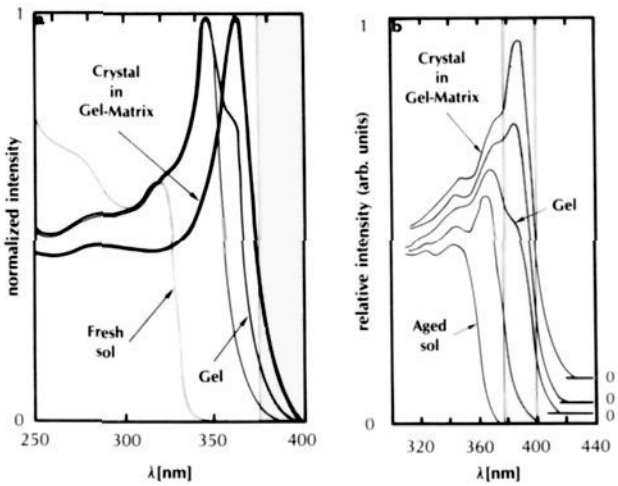

Figure 9. Transition from 0.001 M ZnO sol → 1 M syrup → gel → large crystals (see Figure 11) and corresponding changes in luminescence excitation spectra. (a) Performed with fresh colloid prepared at 0 °C; (b) performed with aged colloid (for details see text); the dark regions represent wavelength range of starting absorption in ZnO bulk crystals at room temperature as known from literature.[26]

in primary clusters (narrow emission band peaking at 350 nm) is seen. If the molarity is raised beyond 0.5 M (not shown in Figure 8), the intensity of this band decreases until this band can no longer be detected in 1 M colloids. In addition, the broad emission band peaking at 500 nm shifts to 560 nm when generated at 320 and 380 nm, respectively (compare Figures 5 and 8). Second, an excitation spectrum generated at 450 nm shows two transitions at 340 and 320 nm, while only the 340-nm peak is seen when generated at 650 nm. The 320-nm peak is not as pronounced in 1 M colloids (compare Figures 4 and 8). Assuming an equilibrium between isolated and aggregated clusters, the following explanation is possible. The presence of mostly isolated clusters (in 0.001 M colloids) and mostly aggregated clusters (in 1 M colloids) seems to result in detection wavelength independence of luminescence spectra. In 0.5 M colloid, the emission of low-energy photons (at 650 nm) is mainly produced through electronic transitions within cluster–cluster aggregates (one peak in excitation spectrum). The emission of high-energy photons (at 450 nm) occurs in both isolated and aggregated primary clusters (two pronounced peaks in excitation spectrum).

Secondary Aggregation Events. Figure 9 shows changes in luminescence excitation spectra during the transition dilute sol → syrup → gel → large crystals. Fresh (part a) and aged (part b) ZnO colloid samples were employed in this process. As in-

troduced above, the forced growth of primary cluster–cluster aggregates produces one intense excitonic transition as the colloids concentrate toward syrups. Additional changes occur upon further concentration to 10–15 M ZnO colloids. These honeylike liquids undergo gelation, which usually takes 1–2 h. Near the gel point, a new excitonic transition is activated. This can be seen as a shoulder at 360 nm and at 390 nm in Figure 9, parts a and b, respectively. The X-ray diffraction patterns of the formed alcogels did not shown a finite size broadening different from the dilute precursor stages. Hence, we attribute the spectroscopic observations to a growth of secondary cluster–cluster aggregates. Although classical[21] and percolation-based[22] theories concerning gelation processes have been proposed, application of these theories to our data goes beyond the purpose of this paper. However, an increasingly popular fractal approach to aggregation and gelation phenomena, as well as to photochemistry on solid surfaces, deserves to be mentioned at this point.[5,23-28]

Recognizing gels physically (they do not flow) is easier than describing them physically, as they represent a boundary between the liquid and solid states. In our reversible alcogel case, one could imagine a giant solid skeleton composed of weakly connected crystallites, surrounded by a continuous ethanol phase. However, the obvious bond formations, producing excitonic transitions on the entire sol–gel processing scale, continue beyond the gel point. The ZnO alcogels start to transform themselves into optically transparent crystals. Ater 12 h the vessels are completely filled with these crystals while the gel network collapses. In fresh samples the crystal growth results in two excitonic peaks at 280 and 360 nm (Figure 9a). In spectra of the aged counterpart, transitions within the primary aggregates still can be seen. Again, one can break apart the crystals in ultrasound followed by further dilution until the original spectra are restored. It is also interesting to note that these consolidation processes change the luminescence color. Although dilute fresh colloids emit blue-turquoise photons, crystallizing alcogels emit green–yellow photons when exposed to UV. These color changes are reversible as well. Additionally, during the alcogel dilution, excitonic transitions at lower eneriges are deactivated faster than those at higher energies. Hence, one may conclude that the larger aggregates are less stable than the smaller ones. A similar conclusion was drawn from photocorrosion studies on CdS colloids.[29]

Figure 10 shows a 5-mL vessel, which contains a ZnO alcogel in early crystal growth stages, exposed to UV light. The results of an optical microscopic investigation of the crystals in the early growth stages are also included. One recognizes trapezoid-based shapes and rodlike shapes (growth along the *c* axis) of different sizes surrounded by their mother liquor. By use of dark-field technique and plane-polarized light, characteristic diffraction patterns were found. When the crystals were rotated relative to the polars, the extinction of color fringes occurred simultaneously throughout the entire sample. This observation is a common test for crystal regularity and provides clear evidence that single crystals are present. Additional proof for the presence of ZnO single crystals has been established by XRD measurement with the crushed ZnO crystal. The sample showed a well-known wurtzite diffraction pattern; and, unlike the small precursor colloidal clusters or alcogels, the XRD line broadening was instrumental. Nevertheless, the detailed optical, chemical, and XRD analysis of the grown ZnO crystals requires further studies and goes beyond the scope of this paper.

Optical Absorption of Aggregates. There are two known quantum mechanical calculations predicting how the energy of the lowest excited state should decrease with increasing ZnO crystallite size.[20,27] In these calculations, Weller et al. described a photogenerated electron–hole pair (exciton) as one body confined in a spherical box with a finite potential wall, using hydrogen-like wave functions. In a slightly more elegant two-body calculations, Brus[27] used a more general wave function incorporating radial correlation between the electron and hole. Brus pointed out that his model describes correctly large crystalline sizes while it fails for extremely small particles (sizes below 3 nm) due to a substantial increase in the kinetic energy of electrons.

By comparing our TEM, X-ray, and luminescence data from our fresh and aged colloids with both models, we note a good agreement with the electron–hole correlation model as shown in Figure 11. The 320- and 350-nm peak maxima from the excitation spectra of dilute colloid samples were taken (labeled as $A_0 \rightarrow A_1$ transitions), rather than the onset values. It seems to be more accurate as this study shows that, even in highly dilute samples, aggregation causes a red shift in the excitation onset without changing the primary cluster size. The horizontal lines in Figure 11 indicate the extent to which activated electronic transitions were shifted (exciton delocalization) as a result of the forced cluster consolidation. The $B_0 \rightarrow B_1$ and $C_0 \rightarrow C_1$ assignments reflect wavelength positions of the highest exciton oscillator strength within primary and secondary cluster–cluster aggregates, respectively. For the primary aggregates in fresh colloids, the excitonic transition at ~350 nm corresponds to a particle size of ~5.5 nm. One can calculate an aggregation number of ~4 primary clusters per aggregate. For the secondary aggregates, the excitonic transition at ~360 nm corresponds to a particle size of ~7 nm, which gives an aggregation number of ~8. On the other hand, for the primary aggregates in aged colloids, again, an aggregation number of ~8 was calculated. However, since the correlation diagram in Figure 11 shows how the wavelength of the lowest excitonic state should increase with increasing diameter of a solid sphere, the use of this plot to determine possible aggregate structures is critical. To clarify the origin of the aggregation-induced spectral shifts and related interparticle interactions requires further work. An intense study of this subject in the future is important as sol–gel-based compact semiconductor films represent potentially interesting materials for use in photoelectrochemical cells and membrane reactors for photocatalytic processes.

Particularly interesting is the 390-nm transition with the associated excitation onset at 430 nm in aged colloids. These values correspond to energy values of 3.2 and 2.9 eV, unlike the values of ~3.3 and 3.1 eV for room-temperature bulk crystals.[26] In other words, the energy range of starting absorption of secondary aggregates in aged ZnO colloids is found to be red shifted compared to room-temperature ZnO bulk crystals. While it is known that yellow, pink, and red ZnO crystals can be grown without doping,[28] the authors did not present the spectroscopic properties and band gap energies of these crystallites.

Another question is the origin of the $X_0 \rightarrow X_1$ transition at 275 nm (Figures 3, 9, and 11), as often seen in freshly prepared ZnO colloids. The following possibilities exist: first, transition into the first and the second excitonic level within 3.5-nm cluster size; second, HOMO–LUMO transitions in two different sizes. A transition into the second excitonic state as proposed from studies on phosphate-stabilized CdS clusters[29] seems to us less probable. Therefore, we believe the 275-nm transition is a HOMO → LUMO transition in very small ZnO clusters composed of less than 200 ZnO molecules ($2R < 2$ nm). HOMO–LUMO transitions have the greatest oscillator strength. It is difficult to imagine a hidden transition into the first excited state (see Figure 9a) while the transition into the second excited state remains visible. On the other hand, extremely small clusters might have

(21) Flory, P. J. *Principles of Polymer Chemistry*; Cornell University Press: Ithaca, NY, 1953.
(22) Zallen, R. *The Physics of Amorphous Solids*; Wiley: New York, 1983.
(23) Avnir, D., Ed. *The Fractal Approach to Heterogeneous Chemistry*; Wiley: New York, 1989, and references therein.
(24) Anpo, M.; Matsuura, T., Eds. *Photochemistry on Solid Surfaces*; Elsevier: New York, 1989.
(25) Abbott, L. F.; Wise, M. B. Dimension of a Quantum-Mechanical Path. *Am. J. Phys.* **1981**, *49*, 37.
(26) Hvedstrup, J.; Skettrup, T. *Phys. Status Solidi* **1973**, *60*, 169. See also: Andres, B. *Z. Phys.* **1962**, *170*, 1.
(27) Brus, L. J. *Chem. Phys.* **1984**, *80*, 4403.
(28) Cimino, A.; Mazzone, G.; Porta, P. Zinc Excess and Distortions in Pure ZnO. *Z. Phys. Chem.* **1964**, *41*, 154–172.
(29) (a) Fischer, Ch. H.; Weller, H.; Katsikas, L.; Henglein, A. *Langmuir* **1989**, *5*, 429–432. (b) Fischer, Ch. H.; Lilie, J.; Weller, H.; Katsikas, L.; Henglein, A. *Ber. Bunsenges. Phys. Chem.* **1989**, *93*, 61–64.

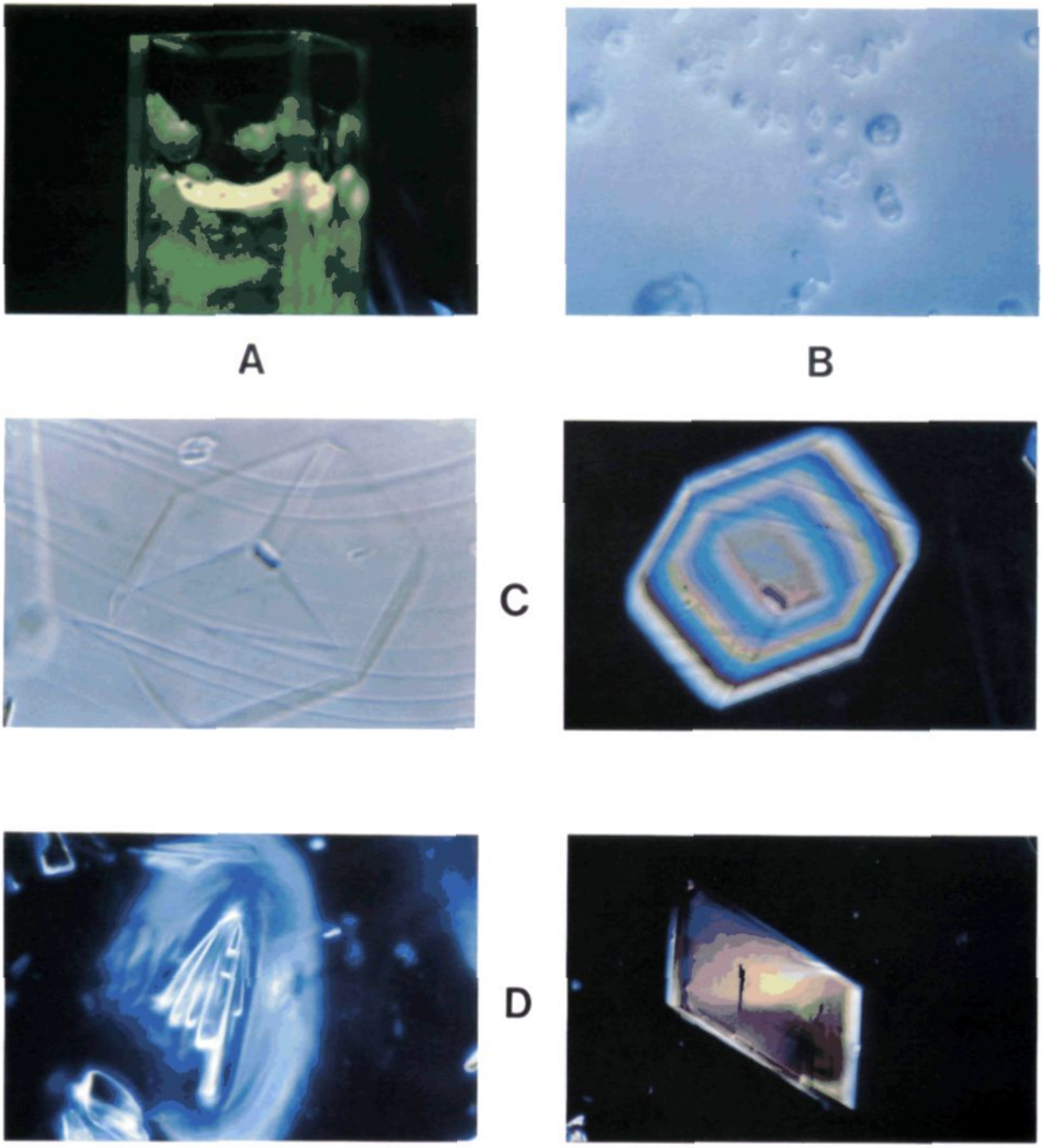

Figure 10. (a) Crystal growth in ZnO alcogels under UV light; (b) bright-field picture from ZnO trapezoids, 4.5 mm horiontal full scale; (c) bright- and dark-field exposure of a trapezoid-based crystal, 1.8-mm horizontal full scale; and (d) rods and trapezoids in dark field, scale as in (c).

more compact wave functions and thus very high oscillator strengths.[27] Larger aggregates appear to have higher densities of electronic states than smaller ones, as discussed in the next section.

Electronic Correlation Diagram. In Figure 12, we propose a *qualitative* MO model based correlation diagram to describe changes in the electronic properties during the aggregate growth. Primary clusters have the largest HOMO–LUMO gap and a low density of electronic states. As they start to combine to give the primary aggregate, bond formations occur due to molecular orbital overlap producing a new HOMO–LUMO gap. As a result, the density of electronic states increases, which causes the $A_0 \rightarrow A_1$ transition in the primary cluster to be screened. Once the primary aggregates start to combine, "secondary" bonding sites form and the $C_0 \rightarrow C_1$ transition appears in the excitation spectra. Secondary aggregates have a smaller HOMO–LUMO gap and a higher density of electronic states when compared with their composite clusters. In the final step, during the crystal growth (development of strong chemical bonds), the aggregates reorganize themselves into lattice order, producing an energy continuum. Thus, the transitions at higher energies are increasingly hidden. This schematic picture might explain the occurrence of structured luminescence excitation spectra not only in ZnO, but also in phosphate-ordered CdS xerogels.[9]

The occurrence of broad, strongly Stokes shifted, emission spectra in all concentration cases is explained as follows. Light absorption in both primary clusters and aggregates generates electron–hole pairs, which are rapidly trapped in shallow and deep surface states. The different lengths of the horizontal bars in Figure 12 indicate that the excitons are more strongly localized in smaller aggregates and deeper traps. The trapped charge carriers tunnel to each other and destroy themselves either in a

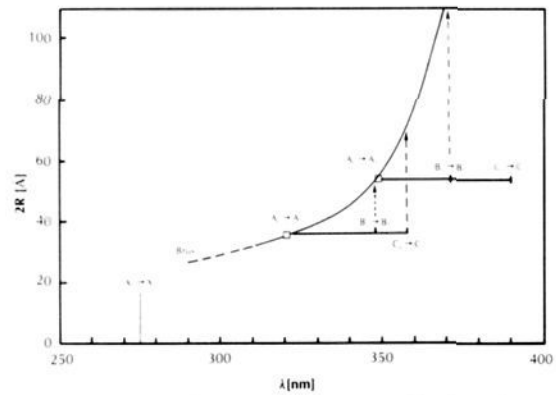

Figure 11. Wavelength of lowest excited state as a function of crystallite size. Solid curve, result of a quantum mechanical calculation by Brus;[2a,27] (□) experimental X-ray crystallite sizes as determined on fresh and aged powder samples and the corresponding $A_0 \rightarrow A_1$ transitions into the lowest excitonic state as seen in Figure 4. $B_0 \rightarrow B_1$, excitonic transitions in primary cluster aggregates; $C_0 \rightarrow C_1$, transitions produced in secondary aggregates.

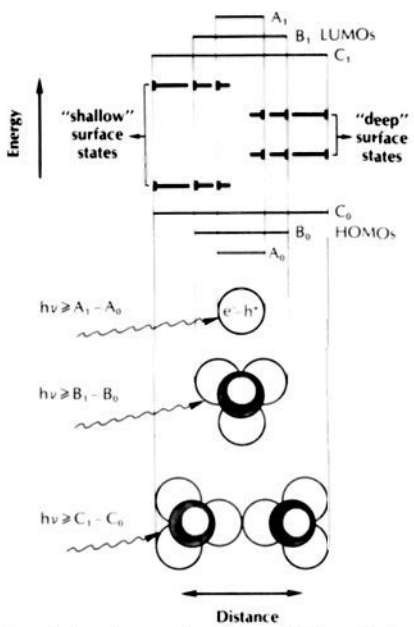

Figure 12. Correlation diagram, based on a MO model, for the growth of ZnO aggregates (see also Figure 11 and text below).

radiationless (coupling to lattice phonons) or in a radiative (emission of photons) manner. Short-distance pairs (in shallow traps (emit photons of higher energy than longer distance pairs (in deep traps). A broad distribution of trap distances can explain the observed broad emission bands.

Again, we underline the qualitative nature of the above proposed diagram. It does not reflect the true aggregation numbers produced in the forced particle consolidation process and, with respect to size-dependent optical changes, is similar to diagrams proposed by Brus[27] and Kormann[13] for continuously increasing solids (without density change). The number of sticking junctions between aggregated clusters and their shape and aggregation number might determine the structure of the aggregates during their growth and, thus, the optical changes within quantum size regime. To account theoretically for such aggregation effects, further quantum mechanical modeling and corresponding interpretation of spectroscopic data is highly desirable.

The increase in luminescence quantum yield from 0.2 to 0.4 during the forced cluster consolidation can be interpreted in a number of ways; for example, removal of water (introduced as $LiOH-H_2O$ by the colloid preparation) as an ethanol–water azeotrope during the rotary evaporation step. Aqueous ZnO

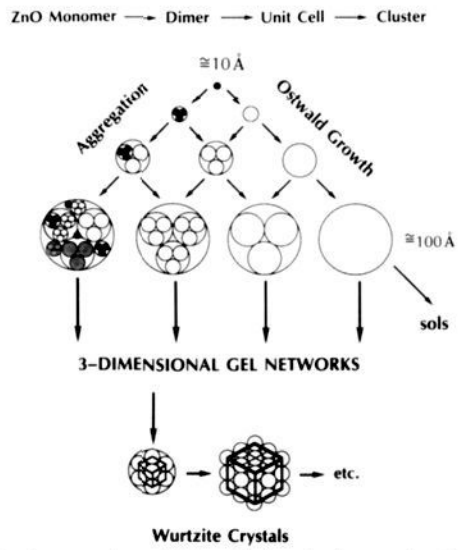

Figure 13. Aggregation and Ostwald ripening in growth of the ZnO crystals.

colloids do not emit as many photons as alcoholic colloids when exposed to UV light. Alternatively, certain surface orbitals, which act as radiationless recombination centers, are consumed by the bond formation that occurs during cluster–cluster aggregation. Nevertheless, neither vacancies due to excess zinc[12] nor oxygen[13] would appear to explain the increase in luminescence quantum yield in our aggregation study.

Aggregation and Ostwald Growth. There are two possible ways of describing the growth of ZnO crystals (see Figure 13). These are Ostwald ripening and aggregation. One question that arises is whether the consolidation of the 3.5- or 5.5-nm clusters into the compact ZnO gel network and crystal state necessitates Ostwald ripening as a precursor step. It could be that, as soon the smallest stable molecular clusters (they may be unit cells) are formed, they rapidly combine to give the next most stable aggregate. The primary aggregates would further rapidly combine to give the next most stable secondary aggregate and so on (see Figure 13). In other words, the primary 3.5- and 5.5-nm clusters, with which we started our consolidation study, actually might be stable aggregates (fragments of the resulting large ZnO crystals). They would be a result of rapid aggregation rather than a result of Ostwald growth. This aggregation model is intimately related the theory of "magic numbers" as proposed by Henglein to describe CdS growth.[1,29] When applied to the growth of ZnO, this theory suggests the association of primary particles composed of m_0 ZnO molecules as follows:

$$m_0Zn^{2+} + n_0O^{2-} \rightarrow (ZnO)_{m0} \quad (2)$$

$$(ZnO)_{m0} + (ZnO)_{m0} \rightarrow (ZnO)_{2m0} \quad (3)$$

Unlike the Ostwald model

$$(ZnO)_{m0} \rightarrow (ZnO)_{m0-1} + Zn^{2+} + O^{2-} \quad (4)$$

$$Zn^{2+} + O^{2-} + (ZnO)_{m+n} \rightarrow (ZnO)_{m+n+1} \quad (5)$$

association would produce a primary particle size distribution peaking at m_0. During the growth, m_0 would be preserved in the form of integer multiples. Hence, the resulting presence of abundant particle size distributions would predict an equally abundant number of electronic transitions in luminescence excitation and UV–vis spectra. The Ostwald model does not explain our structured spectra. However, eq 3 does not provide information as to how the ZnO "particles" are associated. One could imagine that two "balls" stick together or that one larger "ball" is formed that has the same mass. Our proposed aggregation model excludes fusion, although fusion would play an important role during the crystallization of the gel network leading to macroscopic ZnO crystals. To what extent aggregation-based crystal

growth or Ostwald crystal growth occurs (or both overlap) remains to be further worked out. Our experimental results suggest that the Ostwald mechanism should be considered as only one possible approach to the formation of bulk materials.

Summary

A novel sol-gel synthesis of ZnO has been presented. The formation of ZnO crystals was followed spectroscopically throughout the transition from cluster to syrup to alcogel to crystal. Changes in the spectroscopic properties accompanying these transitions were explained in terms of aggregation. Although there are some uncertainties in fitting the data to quantum mechanical models, it seems that the physical idea of a Coulomb-based electron-hole attraction is as effective a model as it is simple. In addition, the presence of primary and secondary aggregate sizes suggests that membranes and films prepared from the ZnO particles would display primary and secondary pore size distributions. Q-ZnO colloids have been successfully applied in fabrication of thin epitaxial ZnO films and ceramic membranes. This will be the subject of another publication. We did not attempt to delve deeply into the complex field of crystal growth. The main purpose of this study is to encourage the use of luminescing semiconductor clusters and corresponding spectroscopic measurement techniques to study aggregation phenomena and crystal growth mechanisms.

Acknowledgment. We gratefully acknowledge the financial support from the NSF (Contract CES-8504276), the U.S. DOE (Contract DE-FC07-88ID12778), and SSI Technologies, Inc. (Janesville, WI). We express our gratitude to Dr. Walt Zeltner for helpful discussions. We enjoyed a very pleasant collaboration with Dr. Grayson Scott (Medical Sciences Department, UW—Madison) during the transmission electron microscopic studies and thank him for his help.

Registry No. ZnO, 1314-13-2; EtOH, 64-17-5.

Twisted Intramolecular Charge-Transfer Fluorescence of Aromatic Amides: Conformation of the Amide Bonds in the Excited States

Isao Azumaya,[†] Hiroyuki Kagechika,[†] Yoshihisa Fujiwara,[‡] Michiya Itoh,[‡] Kentaro Yamaguchi,[§] and Koichi Shudo*,[†]

Contribution from the Faculty of Pharmaceutical Sciences, University of Tokyo, 7-3-1 Hongo, Bunkyo-ku, Tokyo 113, Japan, Faculty of Pharmaceutical Sciences, Kanazawa University, Takara-machi, Kanazawa 920, Japan, and School of Pharmaceutical Sciences, Showa University, Hatanodai, Shinagawa-ku, Tokyo 142, Japan. *Received July 16, 1990*

Abstract: The mechanism of the dual fluorescences of benzanilide (**1**) and *N*-methylbenzanilide (**2**) in methylcyclohexane was investigated. The emission at longer wavelength is composed of one component for **1** (λ_{max} 477 nm) and of one major component (96%, λ_{max} 518 nm) for **2**. Various substitutions on the aromatic rings permit the study of the F_2 fluorescence wavelength and intensity on twisting about the Ar–CO, the Ar–N, and the amide bond (N–CO) itself. Though the ground-state structures of **1** and **2** are very different from each other, the structures of the emitting species of both compounds are considered to be similar. Studies on conformationally restricted derivatives showed that the amide bond must be rotated for the emission of longer wavelength. Quantitative data indicate that the F_2 emissions are generated from excited twisted intramolecular charge-transfer (TICT) species with twisted amide bonds.

Introduction

Benzanilide (**1**) exhibits an anomalous fluorescence with a large Stokes shift that is at longer wavelength than that of its phosphorescence.[1] Generally, such anomalous fluorescence is emitted from a species that is energetically much more stabilized than the primarily formed species. Recent nano- or picosecond studies on the large Stokes-shifted fluorescence have revealed various mechanisms, such as the formation of an intra- or intermolecular excited complex (excimer, exciplex, solvent reorientation, and so forth) or a change of the structure (proton transfer,[2] twisted intramolecular charge transfer,[3] and so forth). However, the emitting mechanism of aromatic anilides including benzanilide (**1**) has seemed to be complicated. In 1971, O'Connell et al. reported that the fluorescence of **1** was observed only in the solid state or in a rigid matrix of EPA (ethyl ether:isopentane:ethanol = 5:5:2 v/v).[1] Furthermore, *N*-phenylisoindolinone, which is a conformationally restricted analogue of **1** containing a five-membered ring system, was shown to emit similarly to **1** even at room temperature in fluid EPA. These results indicated that only quite subtle changes of geometry at the emitting states must be occurring. Recently, Tang et al.[4] and Heldt et al.[5,6] showed that the fluorescence at longer wavelength of **1** in cyclohexane or methylcyclohexane (MCH) could be ascribed to two overlapping mechanisms, that is, proton transfer and twisted intramolecular charge transfer (TICT), using dielectric solvent effects on spectral position, band half-width, and solvent environmental effects. They then sought to confirm these assignments by time-resolved absorption spectroscopy and fluorescence decay dynamics studies.[7] However, their conclusion on the emitting mechanisms was based in part on biexponential fitting of the fluorescence decay curve of **1** and a comparison with the fluorescence of *N*-methylbenz-

[†] University of Tokyo.
[‡] Kanazawa Univeristy.
[§] Showa University.

(1) O'Connell, E. J., Jr.; Delmauro, M.; Irwin, J. *Photochem. Photobiol.* **1971**, *14*, 189-195.
(2) See special issue of "Spectroscopy and dynamics of elementary proton transfer in polyatomic systems": *Chem. Phys.* **1989**, *136*, 153-360.
(3) Rettig, W. *Angew. Chem., Int. Ed. Engl.* **1986**, *25*, 971-988.
(4) Tang, G.-Q.; MacInnis, J. M.; Kasha, M. *J. Am. Chem. Soc.* **1987**, *109*, 2531-2533.
(5) Heldt, J.; Gormin, D.; Kasha, M. *J. Am. Chem. Soc.* **1988**, *110*, 8255-8256.
(6) Heldt, J.; Kasha, M. *J. Mol. Liq.* **1989**, *41*, 305-313.
(7) Heldt, J.; Gormin, D.; Kasha, M. *Chem. Phys.* **1989**, *136*, 321-334.

0002-7863/91/1513-2833$02.50/0